Nano Energy (2016) 22, 396–405

Available online at www.sciencedirect.com

ScienceDirect

journal homepage: www.elsevier.com/locate/nanoenergy

FULL PAPER

# Unbiased solar energy storage: Photoelectrochemical redox flow battery

João Azevedo[a,b], Thorsten Seipp[c], Jens Burfeind[c], Célia Sousa[b], Anders Bentien[d], João Pedro Araújo[b], Adélio Mendes[a,*]

[a]LEPABE-Faculdade de Engenharia, Universidade do Porto, Rua Dr. Roberto Frias, 4200-465 Porto, Portugal
[b]IFIMUP and IN - Institute of Nanoscience and Nanotechnology, Departamento de Física e Astronomia, Faculdade de Ciências da Universidade do Porto, Rua do Campo Alegre, 678, 4169-007 Porto, Portugal
[c]Fraunhofer Institute for Environmental, Safety, and Energy Technology UMSICHT, Osterfelder Street 3, 46047 Oberhausen, Germany
[d]Department of Engineering, Aarhus University, Hangøvej 2, 8200 Aarhus, Denmark

Received 28 October 2015; received in revised form 20 January 2016; accepted 15 February 2016
Available online 22 February 2016

**KEYWORDS**
Redox flow battery;
Solar energy storage;
Tandem device;
Dye-sensitized solar cell;
Cadmium sulfide

**Abstract**
Electricity from renewable energy sources is craving for efficient storage technologies, in particular solar industry, to enable practical small-scale solutions for residential and offices use. The best stationary technology is probably the redox flow batteries. This article proposes the direct conversion of sunlight into electrochemical energy stored in a redox flow battery. A photoelectrochemical cell is used to charge a vanadium redox flow cell (CdS(s)|$V^{3+}$, $VO^{2+}$||$V^{3+}$, $V^{2+}$|Carbon Felt(s), $E^0$=0.6 $V_{NHE}$). A CdS thin film photoelectrode is prepared to directly charge the cell, pairs $V^{3+}/VO^{2+}$. CdS photoanode exhibits competitive photocurrents, when compared to other photoelectrochemical devices, and yields enough photovoltage to charge the vanadium battery up to 75% with no external bias. An overlayer of CdSe improves the performance of CdS with current densities up to ca. 1.4 mA $cm^{-2}$. Finally, a tandem configuration is tested using a dye-sensitized solar cell and a CdS photoanoade creating ~1.3 V of photovoltage. This tandem arrangement proves to charge conventional all vanadium redox cell (DSC/CdS(s)|$VO^{2+}$, $VO_2^+$||$V^{3+}$, $V^{2+}$|Carbon Felt(s), $E^0$=1.2 $V_{NHE}$) without external bias.


## Introduction

The efficient exploitation of renewable energy sources is the only route for long-term energy supply. However,

*Corresponding author.
*E-mail address:* mendes@fe.up.pt (A. Mendes).

http://dx.doi.org/10.1016/j.nanoen.2016.02.029

renewable energy is often intermittent, local in nature [1] and there is an inherent mismatch between production and consumption. If future goals of fully renewable energy sources are to be met it is paramount that efficient storage technologies are developed. Compared to other storage systems, such as conventional batteries, gravity or mechanical-based and supercapacitors, that can be used for the applications requiring moderate energies and high power densities, chemical fuels combine the advantages of ease of transportation and high-energy storage densities [2-4].

For the past two decades, storage in hydrogen through electrolysis of PV electricity or direct photoelectrochemical water splitting has been some of the most investigated technologies for storage of solar energy [5-8]. Much effort was devoted to fabricate and optimize photoelectrochemical (PEC) cells for water splitting offering the prospect of clean, dispatchable, abundant, and affordable energy. However, hydrogen is a very low-density gas requiring high-end technology for storage and transport. Also, its production via PEC cells route still presents many unsolved challenges, in particular low conversion efficiency [9,10]. PEC cells require an abundant semiconductor material with a band gap energy ($E_g$) large enough to split water and a conduction band-edge energy ($E_{cb}$) and valence band-edge energy ($E_{vb}$) that straddle the electrochemical potentials for generation of hydrogen ($E^0_{H^+/H_2}$) and oxygen ($E^0_{O_2/H_2O}$) [9]. This requirement limits the possibilities to a handful of semiconductor materials. Since the positions of both the band edges in many semiconductors and $E^0_{H^+/H_2}/E^0_{O_2/H_2O}$ shift with $-59$ mV per pH unit [2], pH-tuning strategies to match energy levels are not effective.

In a PEC cell, the photo induced free charge carriers migrate to a semiconductor/liquid junction reacting with electroactive species directly at the semiconductor interface. Given the energy efficiency losses at semiconductor/liquid junctions due to the concentration and kinetic overpotentials needed to drive the hydrogen and oxygen evolution reactions, the energy required for photoelectrolysis is frequently reported to have values around 2 eV per electron-hole pair generated [2,11]. Considering the significant amount of research in the field for the past two decades, practical semiconductors solutions that enable unbiased and efficient single photoelectrode solar water splitting appear unlikely.

The use of photoeletrodes for converting solar into electrochemical energy in a redox flow battery (RFB) arrangement is a disruptive approach that allows an efficient storage of solar energy. Contrary to water splitting, where oxidation and reduction potentials are unique, in the case of direct solar charging redox flow batteries it is potentially possible to find two redox pairs for a selected photoelectrode, fitting the redox potentials with the semiconductor band edges. Moreover, the round trip energy efficiency using redox pairs for storing electricity is very high, ca. 85%, compared to hydrogen with round trip energy efficiencies of 20-50% [12]. The direct solar charging of redox flow batteries is then viewed as a premium opportunity for the research on photoelectrochemical cells.

Preliminary experiments using a photoelectrode for charging redox pairs have been reported in the 80 s but limited choice of redox pairs and membrane limitations made the combined PEC and RFB device unable to efficiently convert solar into electrochemical storable energy and research in this topic came to a halt for decades [13,14]. Compared to PEC water splitting, for solar-RFB there are multiple choices of the redox couples given a great flexibility for choosing suitable photoelectrodes. Semiconductors that are unsuitable for water splitting due to thermodynamic potential mismatch or corrosion may now be used for solar-RFB since the choice of redox pairs is quasi-unlimited with redox potentials varying almost continuously [15-17]. Furthermore, most of the charge transfer processes involving redox couples normally used in RFB have faster kinetics since they

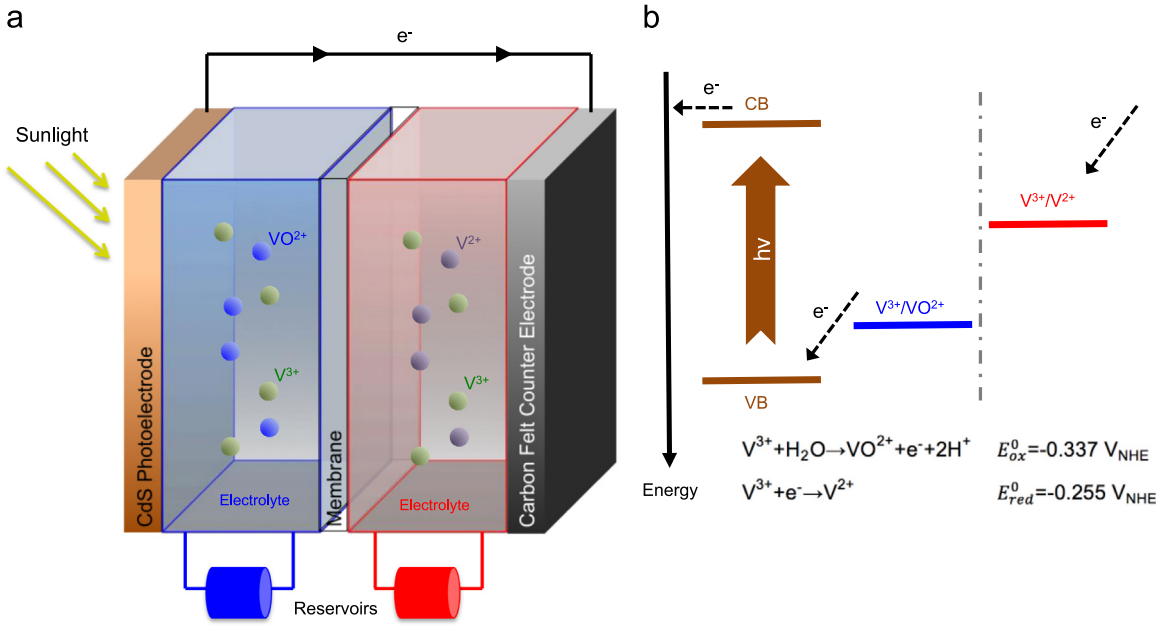


**Figure 1** Schematic diagram of (a) all vanadium solar redox flow battery charged with a CdS photoanode and (b) energy diagram of the system, including the standard redox reactions.

rely on single or double electron transfer processes [15,16,18,19]. Thus, the overall system of solar-RFB is very likely to be more efficient and the direct conversion of sunlight into electrochemical energy may potentially be a cost effective alternative to photovoltaic (PV) charged RFB. The RFB can receive simultaneously charged electrolytes from the PEC panels or electricity from the grid or PV panels and convert it into the chemical energy stored in the charged electrolytes. Sunlight can be used to heat up the electrolytes (thermal solar collector) in a cogeneration arrangement. The heated electrolytes can then heat exchange with sanitary waters and for thermal comfort, where for cooler climates a heat pump may be needed - Figure S1.

While this work was being developed, two different research groups published work on the solar battery concept. Wu et al. combined a dye sensitized $TiO_2$ photoelectrode and a lithium based battery describing the advantages of having a photoassisted battery charging [20,21]. Despite the reported advantages, single photoelectrode unassisted photocharge is highly unlike for the reported system and a tandem arrangement is most probably not beneficial due to the photoanode broad absorption spectrum. Moreover, the energy storage capacity of a lithium based battery is limited by the size of the battery, making this technology unpractical for very large applications. Liu et al. integrated an all vanadium redox flow battery (RFB) with a $TiO_2$ photoelectrode with high Faradaic efficiencies [22,23]. RFBs are easily scalable, display high round trip efficiencies, long lifetimes and acceptable costs for large-scale electrical energy storage, when compared with lithium-based batteries [15,16,24]. The charging measurements of the all vanadium RFB, by Liu et al. were conducted with discharged batteries and a voltage gain of less than 0.05 V is reported [23]. Contrarily to solar water splitting, where the redox potentials of the chemical species in solution are constant during electrochemical reactions (not accounting small pH changes), in RFB an intrinsic electrochemical potential variation is observed governed by the Nernst equation [25]. The battery was charged up to 5% state of charge (SOC); beyond this point more potential is required from the photoanode to charge the battery, which the authors have not demonstrated to be possible with the proposed photoelectrode. Moreover, a $TiO_2$ photoelectrode, which has a wide band gap, can only absorb a small part of the solar spectrum, making $TiO_2$ based devices energy inefficient.

Figure 1a is a schematic representation of the proposed solar RFB that consists in a cadmium sulfide (CdS) semiconductor electrode placed at the negative (photoanode) side of a RFB. The photogenerated electron/hole pairs conduct the necessary redox reactions to charge the battery whereas the charged electrolytes are stored in two external tanks. Given that the photoelectrode provides enough voltage to charge the battery, direct charge can be conducted in a stand-alone device (with no external bias needed). The vanadium electrolytes were selected not only for their good kinetics or reversibility, but also for energy fit with the CdS band gap positioning - Figure 1b. In this work, for the first time, it is demonstrated that the solar RFB, CdS (s)$|V^{3+}$, $VO^{2+}||V^{3+}$, $V^{2+}|$Carbon Felt(s), $E^0 = 0.6\ V_{NHE}$, can be charged up to 75% SOC without any external bias with photocurrents of ca. 1.4 mA $cm^{-2}$. This was possible due to a good match between selected electrolyte and semiconductor. In this work it is intended to prove the possibility to achieve easily unbiased charging of a RFB. In the future other electrolyte/semiconductor combinations can be used to achieve higher efficiencies and energy densities. With the current developments in RFB technology [16,19,26,27] an even larger range of electrolytes could be available for energy fine-tuning between photo absorber and redox pairs.

## Materials and methods

### Substrate preparation

Conducting fluorine doped tin oxide (F:$SnO_2$) glass was used as substrate (Solaronix TCO22-7). FTO-glass was cut into $1 \times 3\ cm^2$ pieces and then cleaned by sonication sequentially in soapy water (15 min), acetone (15 min), ethanol (15 min), and finally in distilled water (15 min).

To obtain reproducible high quality samples, the FTO substrate was delimited with an epoxy resin resistant to high temperatures (Araldite® Super Strength). The active area was measured from photographs of the samples with image analysis software [28], and found to be $0.94\ cm^2 \pm 0.37\ cm^2$.

### CdS thin film fabrication

CdS thin films can be prepared by different methods; here electrodeposition [29] has been chosen because the morphology and nanoparticle size of the films can be easily controlled by e.g. pH, temperature and deposition potential [30-32].

The chosen electrodeposition conditions of the CdS thin films were based on previous reports [33,34] and optimized for the present system. Briefly, CdS thin films were deposited in a plating bath containing 2 mM $CdSO_4$ (99%, Sigma-Aldrich) and 100 mM $Na_2S_2O_3$ (98%, Sigma-Aldrich), with pH adjusted to 2.5 using 2 M $H_2SO_4$ (95-97% Fluka). The bath was kept at 40 °C with stirring throughout the deposition. A three-electrode configuration cell with a ZENNIUM (Zahner Elektrik, Germany) electrochemical workstation was used at a constant potential of −0.8 V for 2 h for most of the samples. The counter-electrode was a 99.9% pure platinum wire (Alfa Aesar, Germany) and the reference electrode was Ag/AgCl/Sat.KCl (Metrohm, Switzerland). After electrodeposition the samples were annealed at 450 °C for 30 min, in ambient atmosphere, under forced air flux. The films had a thickness of ca. 200 nm.

### Under and overlayers deposition

Different configurations were tested in order to improve the performance of the CdS photoelectrodes. Layers of n-type semiconductors were deposited on top of CdS or directly on FTO such as $TiO_2$ and CdSe. Epoxy resin or Teflon® tape was used to cover any exposed FTO substrate and delimit the active area.

Cadmium selenide (CdSe) was electrodeposited from a 2 mM aqueous solution of $SeO_2$ (99.8%, Sigma-Aldrich) in 20 mM $CdSO_4$, at pH=2. Galvanostatic deposition was done with 1 mA $cm^{-2}$ at 30 °C using the same three electrode

configuration as described above. The deposition time was adjusted to 400 s to give a 200 nm thick film.

Titanium dioxide ($TiO_2$) overlayer films were deposited using atomic layer deposition (Beneq TFS 200) at a substrate temperature of 225 °C using titanium isopropoxide (99.99%, Aldrich), at a precursor temperature of 45 °C, and water at room temperature. $TiO_2$ was deposited in pulse mode under a nitrogen flow of 0.250 $L_{STP}$ $min^{-1}$, with a pulse length of 1 s and a purge time of 5 s for $TiO_2$ and a pulse length of 1 s and a purge time of 3 s for water. The growth per cycle of $TiO_2$ corresponded to 0.58 Å $cycle^{-1}$ at 225 °C. The samples were annealed at 500 °C for 15 min.

Underlayer of porous $TiO_2$ (denoted as $TiO_2$ paste) was deposited by doctor blade of a $TiO_2$ paste (Ti-Nanoxide T/SP from Solaronix) followed by drying at 80 °C for 20 min. The samples were annealed at 500 °C for 15 min. The thickness was approximately 5 μm.

Crystalline structure of underlayers and overlayers was checked by X-ray diffraction and energy-dispersive X-ray spectroscopy as described in Section 2.4.

## Thin Film Characterization

The morphology and surface topography of the films was characterized using a high-resolution scanning electron microscope (FEI Quanta 400 FEG ESEM) with a through-the-lens detector for secondary electrons. The acceleration voltage was 15 keV while an in-lens detector was employed with a working distance of about 10 mm. Cross-sectional images were acquired from freshly cleaved samples. The compositions of as-obtained thin films were studied by energy-dispersive X-ray spectrometry (EDAX Genesis X4M).

The crystalline structure of the samples was analyzed by X-ray diffraction (XRD) in a Rigaku MiniFlex 600 diffractometer in the $\theta-2\theta$ geometry using the Cu-Kα line with wavelength $\lambda=1.540593$ Å. The spectra were acquired by moving the detector between $2\theta=20^\circ$ and $2\theta=60^\circ$ at a scan rate of 0.6 deg $min^{-1}$ with a step width of 0.02°. The spectra peaks were fitted with Lorentzian functions to determine the average grain size according to Scherer equation, as described elsewhere [33]. Reflection patterns were matched literature values [29].

UV-vis spectra were obtained on a Shimatzu UV-3600 UV-vis-NIR spectrophotometer, equipped with a 150 mm integrating sphere and using $BaSO_4$ as 100% reflectance standard. A quartz cuvette with path length of 1 cm was used for electrolyte absorption measurements.

## Preparation of vanadium solutions

Vanadium electrolyte solution (AMG-GfE GmbH) containing 1.6 M vanadium in 2 M $H_2SO_4$ was used. The vanadium species were separated in $V^{3+}$ and $VO^{2+}$ using a flow cell at constant potential 1 V (see Eq. (1)), until a clear blue solution was observed on the cathode side and a dark green solution on the anode side, which indicates a good separation of both species. Prior to any test, the initial solutions were screened in the UV-vis-NIR spectrophotometer to check the complete separation of $V^{3+}$ and $VO^{2+}$. The obtained solutions were then diluted to 0.4 M using 2 M $H_2SO_4$.

## Flow cell construction and cycling analysis

The flow cell used had 25 $cm^2$ active membrane area and a thickness of 3 mm. The RFB was assembled in a flow-through configuration. A Nafion™ NM 117 (Quintech) membrane served as the separator. High surface area carbon felt electrodes were used (Sigratherm® GFA5 from SGL Technologies GmbH) with an uncompressed thickness of 6 mm and a specific weight of 500 g $m^{-2}$. The carbon felt was heat-treated at 350 °C for 7 h, in oxygen atmosphere, prior testing for activation. The current collectors were graphite bipolar plates (Sigracet® TF6 from SGL). Contacts to the current collectors were made with nickel-coated copper plates. Battery cycling studies were carried out with a ZENNIUM workstation in a two-electrode configuration. Charge–discharge cycles were recorded galvanostatically, with battery at 0% SOC. All cycling measurements were conducted at current densities of 1 mA $cm^{-2}$. Further, all experiments were performed at room temperature with no active temperature control. Watson Marlow 323 pumps were used to maintain an electrolyte flow rate of 20 mL $min^{-1}$ during cycling measurements. Both reservoirs were argon purged before testing to minimize oxidation of the vanadium species. Charge/discharge cycles of Carbon Felt(s)$|V^{3+}$, $VO^{2+}||V^{3+}$, $V^{2+}|$Carbon Felt(s), $E^o=0.6$ $V_{NHE}$ are represented - Figure S2.

## Solar battery characterization

The photoelectrochemical cell used in the present study is based on previous design [36], and shown in Figure S3. The distance between membrane and each photoelectrode was 1 cm and a Nafion™ NM 117 membrane served as separator. The photoelectrodes were placed as close as possible (~1 mm) from the transparent window to minimize the light absorption from the electrolytes. The carbon felt counter-electrode was bonded to the graphite current collector plate with a carbonized resorcinol resin and no compression is thus needed for obtaining a good electrical contact. The carbonization/pyrolysis process is described elsewhere [37].

For measurements at different SOC, the electrolytes were charged using an electrochemical cell equipped with two carbon felt electrodes. For example, for a standard all vanadium battery, comprising of initial redox species $V^{3+}$ and $VO^{2+}$ (Carbon Felt(s)$|VO^{2+}$, $VO_2^+||V^{3+}$, $V^{2+}|$Carbon Felt(s)), the battery was charged up to 1.2 V until a small current was observed (corresponding to 20% SOC according to Nernst equation-Figure S4) and the electrolyte absorption spectra were measured. Using Beer–Lambert law [38], the concentration of the vanadium species with different oxidation states was estimated and the experimental SOC computed. Given the high concentration of vanadium ions in solution, the electrolyte samples were diluted before determining the absorption.

The current-potential characteristic curves were recorded by linearly sweeping the potential using a ZENNIUM workstation. The measurements were performed in the dark and under simulated sunlight (Newport solar simulator, 150 W Xe lamp, AM 1.5 G, 1000 W $m^{-2}$) at a scan rate of 10 mV $s^{-1}$ in a two-electrode configuration. The light beam was calibrated with a c-Si photodiode. For stability measurements, no external bias was applied and

the photocurrent response was recorded over time. No hydrogen or oxygen bubbles were observed during the experiments.

### Tandem system

To test a tandem configuration of a CdS photoanode with a dye-sensitized solar cell (DSC), a DSC was fabricated as described elsewhere [39]. Briefly, cleaned FTO glasses were immersed in a 40 mM $TiCl_4$ (99.9% Sigma-Aldrich) aqueous solution at 70 °C, for 20 min. Then, the samples were coated with porous $TiO_2$ layer by screen printing a commercial $TiO_2$ paste (Tiscreen printi from Solaronix), followed by drying at 80 °C for 20 min. Finally, the samples were annealed at 500 °C for 15 min in an infrared electrical oven (Nabertherm Gmbh model GF75). After, samples were again treated with 40 mM $TiCl_4$ aqueous solution and annealed at 500 °C for 15 min. The counter electrodes were made from the same cleaned FTO glass, after being drilled with two holes of 1 mm diameter. A commercial platinum based paste (Platisol T/SP from Solaronix®) was applied on the glass substrate by screen-printing followed by annealing at 400 °C for 15 min. Both electrodes were then sealed using a laser assisted glass frit method. Dye (1 mM N719 dye solution) was recirculated for 10 h, electrolyte was inserted in the cell (Iodolyte Z-150 from Solaronix) and the holes sealed using a glass lamella glued to the substrate using a thermo-plastic sealant (Surlyn®, DuPont). In order to insert the DSC inside the electrolyte, the entire cell edge was protected with epoxy resin resistant to high temperatures (Pattex Nural 22). The DSC was placed in the back of the photoanode, with which was connected in series using an electrical wire. The characteristic curves were obtained for both stand-alone DSC and tandem system.

## Results and discussion

Electrodeposited CdS films were 200 nm thick, compact and homogeneous (Figure 2a). The surface morphology of the samples is nanostructured with cauliflower-like features as small as 50 nm (Figure 2b). Depending on the deposition potential, different morphologies were obtained (Figure S5) and the cauliflower-like nanostructured surface was obtained with a deposition potential of −0.8 V. The

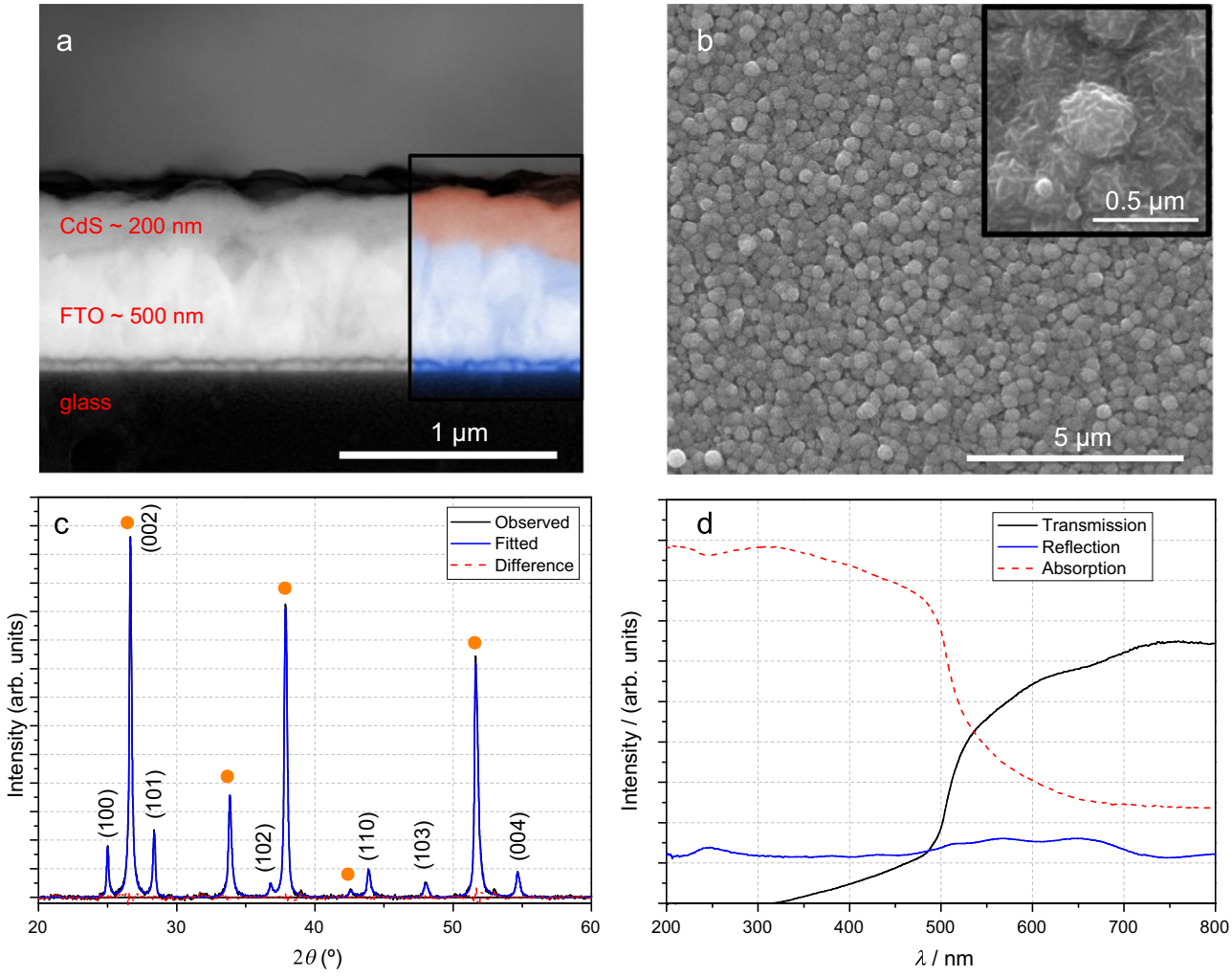


**Figure 2** Cross-sectional (a) and surface (b) SEM micrograph of a CdS photoanode. Inset shows an amplified view of the surface; (c) X-ray diffraction patterns of CdS photoanode. Different crystalline phases are marked with the corresponding miller indexes. Orange circles mark the TCO diffraction peaks; (d) The UV-VIS spectra of CdS thin films.

increased roughness is associated with a better photoactivity of the photoanode [40] and in tests this cauliflower-like nanostructure yielded the best photocurrent performance. The films revealed good adhesion to the FTO glass, imperative for a good electrical performance.

The CdS layer was characterized by X-ray diffraction-Figure 2c; literature values are shown as reference - Table S1 [29]. Each peak was fitted with a Lorentzian function to assess the grain size using Scherer's equation [35]. The fit and difference to measured curves are plotted to verify the quality of the fitting. XRD spectra of CdS films indicate a nanocrystalline size of about 10 nm. Given the small thickness of the samples, the underlying FTO peaks are also visible and are identified in the spectra.

UV-vis spectrophotometry, shown in Figure 2d, was performed to investigate the optical absorption of the films in the range of 200–800 nm. It can be observed that these films exhibit very good light absorption below 500 nm and it transmits most of the light in the 600–800 nm range.

The selected electrolyte for the solar RFB were vanadium aqueous solutions:

$$V^{3+} + H_2O \rightarrow VO^{2+} + e^- + 2H^+ \qquad E^0_{ox} = -0.337V_{NHE} \quad (1)$$

$$V^{3+} + e^- \rightarrow V^{2+} \qquad E^0_{red} = -0.255V_{NHE} \quad (2)$$

This configuration is named V3/V3 from now on. These vanadium species exhibit a standard cell potential of $E^0$=0.6 $V_{NHE}$ (Figure S4). Also, $V^{3+}/V^{2+}$ redox pair is pH independent (Figure S6) offering the possibility to adjust the open circuit voltage (OCV) changing the electrolyte pH up to 2 for better band energy tuning; above this pH some vanadium species may start precipitating. In this work, pH was set to 0 to avoid precipitation and maximize energy density, at the expense of system stability. The OCV was experimentally measured using a carbon-felt electrode on cathode and anode sides, at different SOC values; it was done by applying a constant potential until a small residual current was observed.

Under AM 1.5 illumination, the as-deposited bare CdS produced an unbiased photocurrent as high as 0.47 mA $cm^{-2}$ in a nitrogen-purged 0.4 M $V^{3+}$ electrolyte in 2 M $H_2SO_4$, for completely discharged V3/V3 cell-Figure 3; data shown are from top performing batches. The dark current was negligible up to 0.2 V. Preliminary experiments with a 1.6 M vanadium solution presented smaller photocurrent (~ 0.3 mA $cm^{-2}$) attributed to the electrolyte darker color. The photocurrent onset is at −0.73 V-sufficient to charge the battery up to 90% SOC without external bias, according to Nernst equation (Figure S4).

To confirm the possibility of unbiased charging battery, photocurrent characteristic curves were obtained at different SOCs (Figure 4a). Given the high concentration of vanadium ions in solution, the redox reactions kinetics remained mostly the same across the different SOC, and small differences in fill factors and plateau photocurrents are attributed to sample-to-sample variation. Only after 75% SOC a decrease in photocurrent is observed which was attributed to a depletion of $V^{3+}$ ions at the surface of the photoelectrode and counter-electrode. A shift in the onset is observed as the battery charges. This shift fits perfectly with the Nernst equation: as the battery charges a built in chemical potential is created which requires more voltage

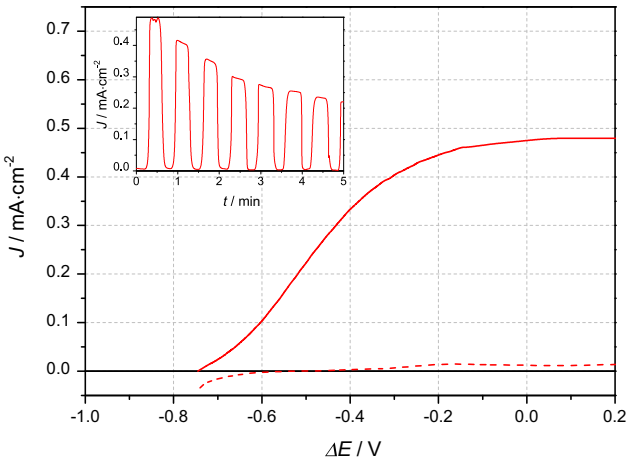


**Figure 3** (a) Photocurrent-photovoltage characteristics under 1.5 AM light and dark conditions (in 0.4 M V3/V3 / 2 M $H_2SO_4$ electrolyte) of the best performing CdS photoanode. Inset shows stability.

to charge the battery further. For this reason, an initial low onset is required to charge the battery to high SOC.

The charging state of the battery was assessed by spectrophotometry. A fully charged and discharged electrolyte sample was analyzed and the absorption spectra were according to literature: $V^{3+}$ showed absorption peaks at 400 nm and 600 nm and $VO^{2+}$ solution at 760 nm, Figure 4b. Starting from a complete discharged state, the battery was charged during equal time intervals at 0 V bias, under continuous 1.5 AM illumination, using several CdS samples. Absorption spectra of the anolyte were taken at each interval and a clear change from $V^{3+}$ to $VO^{2+}$ is observed over time.

The charging was confirmed from the absorption data assuming a linear relationship between concentration and the 760 nm absorption peak of $VO^{2+}$ [38]. From Lambert-Beer law, using 18.46 as $VO^{2+}$ molar absorptivity at 760 nm, the produced amount of $VO^{2+}$ was estimated. After passing ~0.6 C through the photoanode under continuous illumination, an amount of 0.13 mM of $VO^{2+}$ was computed (total electrolyte volume of 14 ml). A conversion rate of ~0.1 mM $h^{-1}$ for $VO^{2+}$ was estimated.

To improve performance it was attempted to coat the photoelectrode with an overlayer. Here it is important that it has a staggered type-II band offset when interfaced with CdS. This ensures that charge carriers are injected in the correct direction for the desired reactions i.e. holes to the electrolyte and electrons to the counter electrode. This is the case of some n-type semiconductors with sufficiently low conduction band edge. Secondly, the layer should have a catalytic activity that promotes the charging reaction (Eq. (1)). Finally, no corrosive side reactions should occur at potentials within the bandgap potential range or at least have sufficiently low corrosion kinetics. Among n-type semiconductors CdSe and $TiO_2$ meets these criteria and were selected to be tested.

Table 1 summarizes the PEC response produced by the two protected photoelectrodes. The maximum photocurrent corresponds to the photocurrent density at 0 V during the linear sweep voltammetry, corrected by the dark current. The stability was assessed over 5 min with

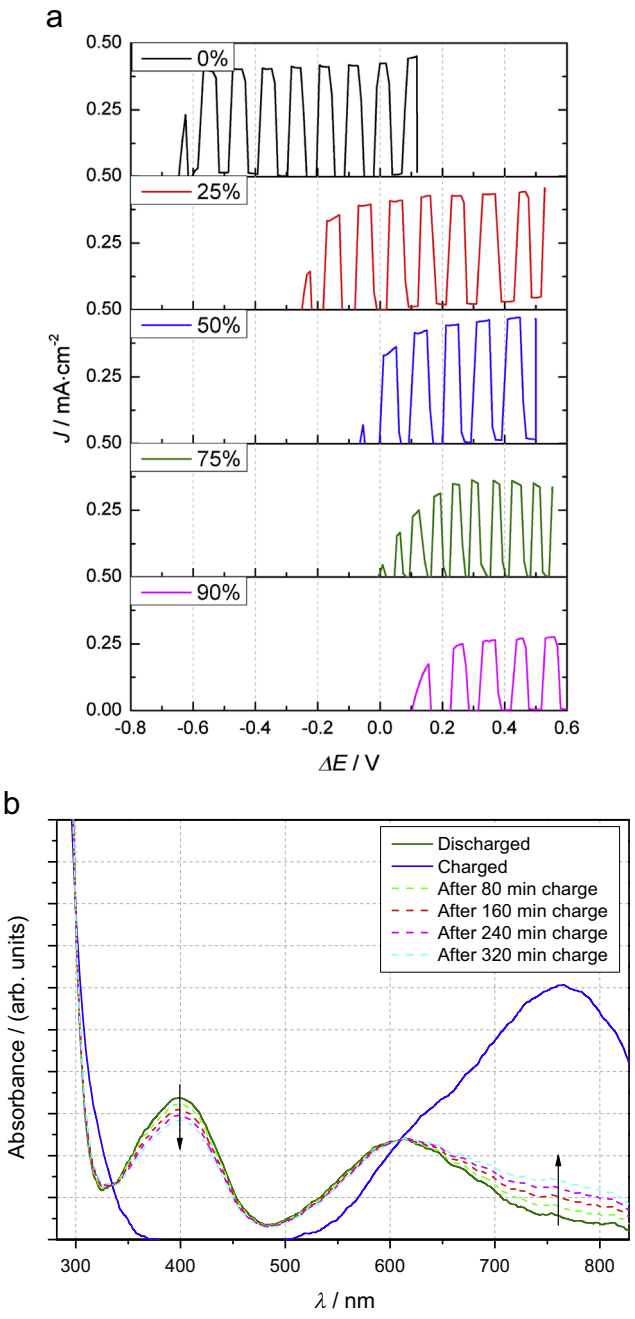


**Figure 4** (a) Photocurrent-photovoltage characteristics under chopped 1.5 AM light CdS photoanode at different SOC values in V3/V3; (b) Absorption spectra of $V^{3+}$-$VO^{2+}$ mixtures at different SOC and for the parent $V^{3+}$ and $VO^{2+}$ solutions.

chronoamperometric measurements at 0 V and chopped light. The final photocurrent density ($J$) was compared with the initial photocurrent density ($J_0$).

$TiO_2$ is a well-tested material as a protective layer for other semiconductors [5,41,42], as well as for CdS [43]. It is stable in a wide range of pH values in aqueous environments and it can be deposited in a conformal and dense layer by atomic layer deposition. Despite previous reports using $TiO_2$ as protective layer of CdS, the low $E_{vb}$ of $TiO_2$ (Figure S7) imposes an undesired potential step for holes diffusion to the electrolyte, thus a resistive behavior is observed. In an attempt to reduce the resistive behavior, very thin layers of $TiO_2$ (5 nm) were tested, however, without improved performance (results not shown).

CdSe, on the other hand, creates a favorable potential step when in contact with CdS [44]. In fact, CdS/CdSe structure is widely studied [29,45-47]. With a band gap of 1.7 eV, good conductivity and light absorption, CdSe has been studied for improving both CdS onset potential and photocurrent. Also, anodic decomposition potential [48] lies below the vanadium oxidation potential implying that CdSe should be more stable than CdS in vanadium electrolytes [29,44,45].

The optimized CdS/CdSe photoelectrode showed an onset at $-0.67$ V and a photocurrent of 1.4 mA $cm^{-2}$ at 0 V bias (Figure 5). CdSe protected samples displayed better stabilities (up to 5 min); but given the extreme pH conditions this still needs to be improved. A stable device can be achieved using sacrificial reagents [49] in the electrolyte but it is not the scope of this work, which solely intends to demonstrate the charge of the vanadium battery with no bias.

The open circuit potential of a RFB is directly related to the energy density it can provide. Open circuit potentials depend on different parameters according to Nernst equation but the standard redox potential is the predominant factor. Most of the commercial redox flow batteries have open circuit potentials over 1 V. The tested photoelectrodes provide insufficient photopotential to charge such a RFB without external bias. The necessary extra voltage can be obtained with a tandem system, placing a PV cell aligned with the photoelectrode [50-52]. The PV cell in front of the photoanode generates an extra bias that is added to the photovoltage of the photoelectrode, provided that enough light reaches the photoanode through the PV cell. A schematic representation of the proposed system is given in Figure 6a. The selected PV technology was a dye sensitized solar cell since it can be made semi-transparent and it is fabricated from low cost and environmentally safe components. The semiconductor samples with lower onset potential were selected, in this case CdS.

As a higher energy density battery the following electrolytes were selected (named V3/V4 from now on):

$$VO^{2+} + H_2O \rightarrow VO_2^{+} + e^{-} + 2H^{+} \qquad E^0_{ox} = -0.991 V_{NHE} \tag{3}$$

$$V^{3+} + e^{-} \rightarrow V^{2+} \qquad E^0_{red} = -0.255 V_{NHE} \tag{4}$$

The DSC cell used had 4 $cm^2$ active area with an open circuit potential of 0.66 V, a short circuit current of $\approx$2.7 mA $cm^{-2}$ and a fill factor of 41% - see Figure S8a; a CdS photoanode matching the useful area of the DSC, 4 $cm^2$, was prepared. The low current density of the DSC cell was attributed to the thin, semitransparent, photoelectrode while the low fill factor was assigned to the large active area that promotes recombination [39]. The selected dye was N719 (Solaronix), which gives a reddish color to the DSC and high absorption across the visible range.

Given that the DSC has the widest absorption range - Figures 2d and S8b - The DSC was placed on the backside of the photoanode. This configuration originated higher photocurrents, in the range of 1 mA $cm^{-2}$ and photopotentials ca. 1.3 V (Figure 6b); a SOC of 70% could be achieved.

**Table 1** Summary of PEC performance for the different ALD layers investigated.

| Sample ID | Anode/Cathode | Configuration | $J$ at 0 V (mA cm$^{-2}$) | $J/J_0$ after 5 min at 0 V (%) |
|---|---|---|---|---|
| 1 | Anode | 200 nm CdS | 0.47 | 46 |
| 2 | Anode | 200 nm CdS/200 nm CdSe | 1.40 | 86 |
| 3 | Anode | 200 nm CdS/200 nm CdSe[a] | 0.66 | 42 |
| 4 | Anode | $TiO_2$[b]/ 200 nm CdS/200 nm CdSe | 0.12 | 63 |
| 5 | Cathode | 200 nm CdS/200 nm CdSe/100 nm $TiO_2$[c] | −1.9 | 47 |
| 6 | Anode | 200 nm CdS/200 nm CdSe/100 nm $TiO_2$[c] | 0.4 | 26 |

[a]Back illumination.
[b]Deposited from $TiO_2$ paste.
[c]Deposited using atomic layer deposition.

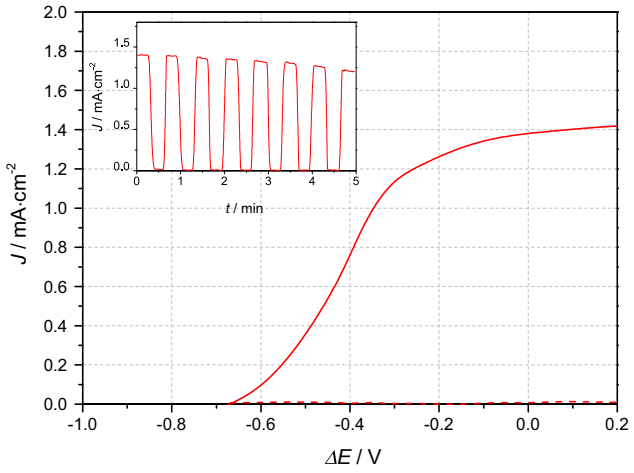


**Figure 5** Photocurrent-photovoltage characteristics of the best CdS/CdSe sample. Inset shows stability.

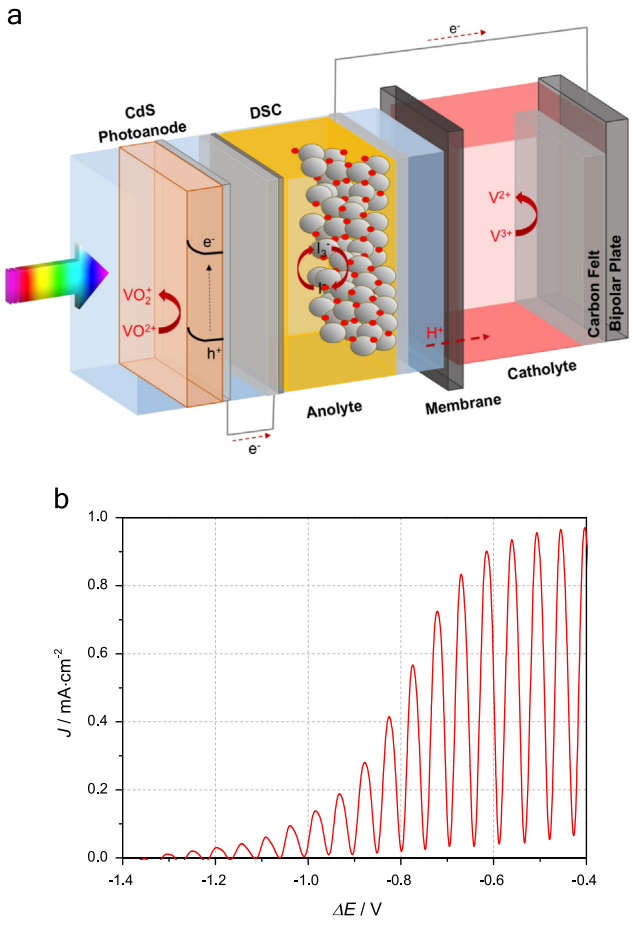


**Figure 6** (a) Schematic representation of a tandem device comprising a DSC and a CdS photoanode to charge a vanadium RFB; (b) Photocurrent-photovoltage characteristics of a tandem system composed by CdS(s)/DSC|$VO^{2+}$, $VO_2^+$||$V^{3+}$, $V^{2+}$|Carbon Felt(s).

## Conclusions

In this work we demonstrated the possibility of storing solar energy in a simple way using a vanadium redox flow battery (RFB) and a CdS photoanode; unbiased charged of a solar-RFB (CdS(s)|$V^{3+}$, $VO^{2+}$||$V^{3+}$, $V^{2+}$|Carbon Felt(s), $E^0$=0.6 $V_{NHE}$) was achieved. A good semiconductor/electrolyte match was achieved allowing the unbiased solar charge of a RFB up to high state of charge (SOC). CdSe protective over layer had a twofold increase with photocurrents up to 1.4 mA cm$^{-2}$ with no external bias. A tandem system battery using a dye-sensitized solar cell was also studied to provide necessary photovoltage to charge a standard all vanadium redox flow (DSC/CdS(s)|$VO^{2+}$, $VO_2^+$||$V^{3+}$, $V^{2+}$|Carbon Felt(s), $E^0$=1.2 $V_{NHE}$); in this configuration, the observed photocurrent was 1 mA cm$^{-2}$.

Given the acidic nature of the electrolytes (pH ≈ 0), the photoanodes are still limited by their long-term stability. To improve further the performance of the proposed solar-RFB system, the CdS/CdSe junction should be further optimized to produce more reproducible photoelectrodes displaying higher photopotentials, currents and stability. Another option is reduced graphene oxide, that have been proven useful in minimizing CdS photocorrosion [53]. It is anticipated that new approaches will be proposed and photoelectrodes able to delivery higher current densities and photopotentials will be soon available. For example, organic alkaline electrolytes are currently being tested that allow the use of stable semiconductors such as hematite.

## Acknowledgments

J. Azevedo and C. Sousa are grateful to the FCT SFRH/BD/79207/2011 PhD grant and postdoctoral grant SFRH/BPD/82010/2011, respectively. A. Bentien acknowledges the Danish Council for Independent Research (Technology and Production Sciences, Grant # 4005-00517B) for funding. This work was supported by research project BI-DSC (grant agreement no. 321315) funded by European Research Council. We also thank José Nogueira (LEPABE) for DSC fabrication, Dr. Verena Stockhausen (LEPABE) and João Barros for graphical design.

## Appendix A. Supplementary material

Supplementary data associated with this article can be found in the online version at http://dx.doi.org/10.1016/j.nanoen.2016.02.029.

## References

[1] H. Lund, Energy 32 (2007) 912–919.
[2] R. van de Krol, M. Gratzel, Photoelectrochemical Hydrogen Production, Springer Science & Business Media, New York, 2011.
[3] T.N. Murakami, N. Kawashima, T. Miyasaka, Chem. Commun. 26 (2005) 3346.
[4] M. Skunik-Nuckowska, K. Grzejszczyk, P.J. Kulesza, L. Yang, N. Vlachopoulos, L. Häggman, E. Johansson, A. Hagfeldt, J. Power Sources 234 (2013) 91–99.
[5] J. Azevedo, L. Steier, P. Dias, M. Stefik, C.T. Sousa, J.P. Araujo, A.M. Mendes, M. Gratzel, S.D. Tilley, Energy Environ. Sci. 7 (2014) 4044–4052.
[6] T. Zhu, M.N. Chong, Nano Energy 12 (2015) 347–373.
[7] J.Y. Kim, G. Magesh, D.H. Youn, J.-W. Jang, J. Kubota, K. Domen, J.S. Lee, Sci. Rep. 3 (2013) 2681.
[8] M. Zhong, T. Hisatomi, Y. Kuang, J. Zhao, M. Liu, A. Iwase, Q. Jia, H. Nishiyama, T. Minegishi, M. Nakabayashi, N. Shibata, R. Niishiro, C. Katayama, H. Shibano, M. Katayama, A. Kudo, T. Yamada, K. Domen, J. Am. Chem. Soc. 137 (2015) 5053–5060.
[9] O.V. Marchenko, S.V. Solomin, Int. J. Hydrog. Energy 40 (2015) 3801–3805.
[10] J.R. McKone, N.S. Lewis, H.B. Gray, Chem. Mater. 26 (2014) 407–414.
[11] M.G. Walter, E.L. Warren, J.R. McKone, S.W. Boettcher, Q. Mi, E.A. Santori, N.S. Lewis, Chem. Rev. 110 (2010) 6446–6473.
[12] H. Chen, T.N. Cong, W. Yang, C. Tan, Y. Li, Y. Ding, Prog. Nat. Sci. 19 (2009) 291–312.
[13] M. Sharon, P. Veluchamy, C. Natarajan, D. Kumar, Electrochim. Acta 36 (1991) 1107–1126.
[14] S. Licht, G. Hodes, R. Tenne, J. Manassen, Nature 326 (1987) 863–864.
[15] A.Z. Weber, M.M. Mench, J.P. Meyers, P.N. Ross, J.T. Gostick, Q. Liu, J. Appl. Electrochem. 41 (2011) 1137–1164.
[16] W. Wang, Q. Luo, B. Li, X. Wei, L. Li, Z. Yang, Adv. Funct. Mater. 23 (2012) 970–986.
[17] S. Er, C. Suh, M.P. Marshak, A. Aspuru-Guzik, Chem. Sci. 6 (2015) 885–893.
[18] B. Yang, L. Hoober-Burkhardt, F. Wang, G.K. Surya Prakash, S. R. Narayanan, J. Electrochem. Soc. 161 (2014) A1371–A1380.
[19] B. Huskinson, M.P. Marshak, C. Suh, S. Er, M.R. Gerhardt, C. J. Galvin, X. Chen, A. Aspuru-Guzik, R.G. Gordon, M.J. Aziz, Nature 505 (2015) 195–198.
[20] M. Yu, X. Ren, L. Ma, Y. Wu, Nat. Commun. 5 (2014) 1–17.
[21] M. Yu, W.D. McCulloch, D.R. Beauchamp, Z. Huang, X. Ren, Y. Wu, J. Am. Chem. Soc. 137 (2015) 8332–8335.
[22] D. Liu, Z. Wei, C.-J. Hsu, Y. Shen, F. Liu, Electrochim. Acta 136 (2014) 435–441.
[23] Z. Wei, D. Liu, C. Hsu, F. Liu, Electrochem. Commun. 45 (2014) 79–82.
[24] P. Alotto, M. Guarnieri, F. Moro, Renew. Sust. Energ. Rev 29 (2014) 325–335.
[25] K.W. Knehr, E.C. Kumbur, Electrochem. Commun. 13 (2011) 342–345.
[26] N. Arroyo-Curras, J.W. Hall, J.E. Dick, R.A. Jones, A.J. Bard, J. Electrochem. Soc. 162 (2014) A378–A383.
[27] K. Lin, Q. Chen, M.R. Gerhardt, L. Tong, S.B. Kim, L. Eisenach, A.W. Valle, D. Hardee, R.G. Gordon, M.J. Aziz, M.P. Marshak, Science 349 (2015) 1529–1532.
[28] Rasband, W.S., ImageJ, U. S. National Institutes of Health, Bethesda, Maryland, USA, ⟨⟨http://imagej.nih.gov/ij/⟩⟩, 1997–2014.
[29] C. Lu, L. Zhang, Y. Zhang, S. Liu, G. Liu, Appl. Surface Sci. 319 (2014) 278–284.
[30] M. Takahashi, S. Hasegawa, M. Watanabe, T. Miyuki, S. Ikeda, K. Iida, J. Appl. Electrochem. 32 (2002) 359–367.
[31] G. Sasikala, R. Dhanasekaran, C. Subramanian, Thin Solid Films 302 (1997) 71–76.
[32] J. Azevedo, C.T. Sousa, J. Ventura, A. Apolinário, A. M. Mendes, J.P. Araujo, Mater. Res. Express 1 (2014) 1–16.
[33] F. Goto, K. Shirai, M. Ichimura, Sol. Energ. Mater. Solar Cells 50 (1998) 147–153.
[34] E. Fatás, R. Duo, P. Herrasti, F. Arjona, E. Garcia-Camarero, J. Electrochem. Soc. 131 (1984) 2243–2246.
[35] J. Azevedo, C.T. Sousa, A.M. Mendes, J.P. Araujo, J. Nanosci., Nanotech 12 (2012) 9112–9117.
[36] T. Lopes, P. Dias, L. Andrade, A.M. Mendes, Sol. Energy Mater. Solar Cells 128 (2014) 399–410.
[37] S.C. Rodrigues, R. Whitley, A.M. Mendes, J. Membr. Sci. 459 (2014) 207–216.
[38] D.N. Buckley, X. Gao, R.P. Lynch, N. Quill, M.J. Leahy, J. Electrochem. Soc. 161 (2014) A524–A534.
[39] J. Maçaira, L. Andrade, A.M. Mendes, RSC Adv. 4 (2014) 2830–2844.
[40] S.D. Tilley, M. Cornuz, K. Sivula, M. Gratzel, Angew. Chem. Int. Ed. 49 (2010) 6405.
[41] S.D. Tilley, M. Schreier, J. Azevedo, M. Stefik, M. Graetzel, Adv. Funct. Mater. 24 (2014) 303–311.
[42] X. Li, P.S. Bassi, P. Boix, Y. Fang, L.H. Wong, ACS Appl. Mater. Interfaces 7 (2015) 16960–16966.
[43] A.S. Aliev, M.N. Mamedov, M.T. Abbasov, Inorg. Mater. 45 (2009) 965–967.
[44] Y.-L. Lee, C.-F. Chi, S.-Y. Liau, Chem. Mater. 22 (2010) 922–927.
[45] S. Cheng, W. Fu, H. Yang, L. Zhang, J. Ma, H. Zhao, M. Sun, L. Yang, J. Phys. Chem. C 116 (2012) 2615–2621.
[46] H.-S. Rao, W.-Q. Wu, Y. Liu, Y.-F. Xu, B.-X. Chen, H.-Y. Chen, D. Kuang, C.-Y. Su, Nano Energy 8 (2014) 1–8.
[47] Y.-F. Xu, W.-Q. Wu, H.-S. Rao, H.-Y. Chen, D. Kuang, C.-Y. Su, Nano Energy 11 (2015) 621–630.
[48] S. Chen, L.-W. Wang, Chem. Mater. 24 (2012) 3659–3666.
[49] X. Wang, G. Liu, G.Q. Lu, H.-M. Cheng, Int. J. Hydrog. Energy 35 (2010) 8199–8205.
[50] X. Shi, K. Zhang, K. Shin, M. Ma, J. Kwon, I.T. Choi, J.K. Kim, H. K. Kim, D.H. Wang, J.H. Park, Nano Energy 13 (2015) 182–191.
[51] D. Gurudayal, M.H. Sabba, L.H. Kumar, J. Wong, M. Barber, N. Gratzel, Mathews, Nano Lett. 15 (2015) 3822–3839.
[52] F.F. Abdi, L. Han, A.H.M. Smets, M. Zeman, B. Dam, R. van de Krol, Nat. Commun. 4 (2013) 1–18.
[53] Y. Tang, X. Hu, C. Liu, Phys. Chem. Chem. Phys. 16 (2014) 25321–25329.

**João Azevedo** obtained a master's degree in Experimental Physics at Porto University, Portugal, in 2011. Currently he is a Physics PhD candidate at Porto University and researching on solar energy storage both at LEPABE, Laboratory for Process Engineering, Environment, Biotechnology and Energy and IFIMUP-IN, Institute of Nanoscience and Nanotechnology. His research centers on the production of solar fuels, with a new photoeletrode development to improve the efficiency of water splitting processes and solar batteries.

**Thorsten Seipp** (born 1986) studied Chemical Engineering in Dortmund. His Diploma Thesis dealed with scale-up of Redox Flow Batteries. Since 2011 he is scientific researcher at Fraunhofer Institute UMSICHT in Oberhausen with focus on redox-flow-batteries. Since 2015 he is furthermore managing director of Volterion GmbH, a spin-off company of Fraunhofer, which produces and sells compact redox-flow-stacks and batteries for decentralized energy storage.

**Jens Burfeind** graduated in Chemistry. He exhibits over 13 years experience in electrochemistry. From the year 2000 he developed fuel cells and electrolyzer at h2-interpower. The last 6 years Dr. Burfeind was head of high temperature PEM working Group at center for fuel cell technology (ZBT). From March 2011 to February 2012 he worked at ReVolt GmbH in the field of zinc air batteries. Since March 2012 Dr. Burfeind works at Fraunhofer Institute UMSICHT as group manager for Electrochemical Storage and Processes. He is responsible for the Vanadium-Redox-Flow Battery development and other electrochemical processes especially in unconventional solvents.

**Célia Sousa** is specialized in nanoscience and nanotechnology and her interdisciplinary research has been mainly focused on the fabrication of nanostructures using top-down methods for biomedical and fuel cells technological applications. She completed her PhD degree in Physics-Nanotechnology in 2011 and has an h-factor of 13, published 48 papers in international peer review journals. She is also author of an invited review article, 2 book chapters and 9 proceedings. Her research led to 3 invited talks, 23 oral presentations and 30 posters in international conferences.

**Anders Bentien** is a permanent staff member at the Department of Engineering of AU section for Bio- & Chemical Engineering. He obtained his Ph.D. in Physics in 2004 at Max Planck Institute for Chemical Physics of Solids of Dresden Technical University. Current research topics within membranes and energy conversion include synthesis/characterization of ion conducting polymer membranes for electrochemical energy conversion applications, electrochemical compressors, redox flow batteries and solar charging of redox flow battery electrolytes with photoelectrochemical cells.

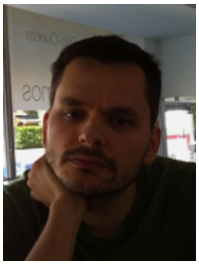

**J. P. Araújo** obtained his PhD in Physics at the University of Porto in 2002 and became Assistant Professor at the Physics and Astronomy Department at the Faculty of Sciences of University of Porto in the same year. He is now Vice-President of IFIMUP-IN, Institute of Nanoscience and Nanotechnology and counts with over 200 papers in international journals. He has relevant contributions in the field of magnetic intermetallics and oxides, and recently, in new phenomena and new technologies based on the magnetism of nanostructured materials.

**Adélio Mendes** is full professor at FEUP and researcher at LEPABE, where he leads the Energy, Processes and Products area. His publications include over 250 papers in peer-reviewed scientific journals and 5 reviews or invited book chapters. He is the inventor or co-inventor of over 20 patents and authored one book. Prof. Mendes is presently the coordinator of project BeingEnergy (Grant agreement no: 303476), project BI-DSC (advanced research grant from ERC) and GOTSolar (Grant agreement no: 687008). He was awarded with Air Products Faculty Excellence Award (2011), ACP Diogo Vasconcelos (2011) and Solvay & Hovione Innovation Challenge 2011 (SHIC'11) prizes.